Synthesis and preclinical evaluation of the CRTH2 antagonist [^{11}C]MK-7246 as a novel PET tracer and potential surrogate marker for pancreatic beta-cell mass

Jonas Eriksson[a*], Tamal Roy[a], Supaporn Sawadjoon[a], Kim Bachmann[a], Christian Sköld[a], Mats Larhed[b], Jan Weis[c], Ram Kumar Selvaraju[a], Olle Korsgren[d], Olof Eriksson[b], Luke R. Odell[a*]

[a] *Department of Medicinal Chemistry, Uppsala University, Uppsala, Sweden*
[b] *Department of Medicinal Chemistry, Science for Life Laboratory, Uppsala University, Uppsala, Sweden*
[c] *Department of Surgical Sciences, Uppsala University, Uppsala, Sweden*
[d] *Department of Immunology, Genetics and Pathology, Uppsala University, Uppsala, Sweden*

**Corresponding authors: Department of Medicinal Chemistry, BMC, Uppsala University, Box-574, SE-75123 Uppsala, Sweden, jonas.eriksson@ilk.uu.se; luke.odell@ilk.uu.se*

Abbreviated title: Synthesis and preclinical evaluation of the CRTH2 antagonist [^{11}C]MK-7246

Keywords: MK-7246, CRTH2, GPR44, Beta-cell mass, Diabetes, PET, Carbon-11

ABSTRACT

Introduction: MK-7246 is a potent and selective antagonist for chemoattractant receptor-homologous molecule expressed on T_h2 cells (CRTH2). Within the pancreas CRTH2 is selectively expressed in pancreatic β-cells where it is believed to play a role in insulin release. Reduction in β-cell mass and insufficient insulin secretion in response to elevated blood glucose levels is a hallmark for type 1 and type 2 diabetes. Reported here is the synthesis of [^{11}C]MK-7246 and initial preclinical evaluation towards CRTH2 imaging. The aim is to develop a method to quantify β-cell mass with PET and facilitate non-invasive studies of disease progression in individuals with type 2 diabetes.

Methods: The precursor *N*-desmethyl-*O*-methyl MK-7246 was synthesized in seven steps and subjected to methylation with [^{11}C]methyl iodide followed by hydrolysis to obtain [^{11}C]MK-7246 labelled in the *N*-methyl position. Preclinical evaluation included *in vitro* radiography and

immune-staining performed in human pancreatic biopsies. Biodistribution studies were performed in rat by PET-MRI and in pig by PET-CT imaging. The specific tracer uptake was examined in pig by scanning before and after administration of MK-7246 (1 mg/kg). Predicted dosimetry of [^{11}C]MK-7246 in human males was estimated based on the biodistribution in rat.
Results: [^{11}C]MK-7246 was obtained with activities sufficient for the current investigations (270±120 MBq) and a radiochemical purity of 93±2%. The tracer displayed focal binding in areas with insulin positive islet of Langerhans in human pancreas sections. Baseline uptake in pig was significantly reduced in CRTH2-rich areas after administration of MK-7246; pancreas (66% reduction) and spleen (88% reduction). [^{11}C]MK-7246 exhibited a safe human predicted dosimetry profile as extrapolated from the rat biodistribution data.
Conclusions: Initial preclinical *in vitro* and *in vivo* evaluation of [^{11}C]MK-7246 show binding and biodistribution properties suitable for PET imaging of CRTH2. Further studies are warranted to assess its potential in β-cell mass imaging and CRTH2 drug development.

1 **Introduction**

The chemoattractant receptor-homologous molecule expressed on T_h2 cells (CRTH2), also designated as GPR44, Prostaglandin D_2 receptor 2 (PTGDR2) or CD294, is a relatively recently discovered[1-3] G-protein-coupled receptor that binds to the endogenous ligand prostaglandin D_2. The most well-known consequences of this binding action are induction of the pro-inflammatory T_H2 cytokines IL4, IL5 and IL13,[4] stimulation and activation of T_H2 lymphocyte, eosinophil and basophil migration[3, 5] as well as inhibition of T_H2 lymphocyte apoptosis.[6] These processes have primarily been linked to allergic inflammation and numerous CRTH2 antagonists have entered clinic development for the treatment of asthma and other allergic disorders.[7, 8] In addition, it has been shown that within pancreas CRTH2 is selectively expressed in pancreatic β-cells[9] and initial studies indicate a role in insulin release (unpublished data). Reduction in β-cell mass (BCM) can lead to insufficient insulin secretion in response to elevated blood glucose levels, a hallmark of Type 1 and Type 2 Diabetes (T1D/T2D). However, BCM can currently only be measured by highly invasive pancreatic biopsies and the progression of BCM loss during the course of diabetes development in individuals is therefore largely unknown. Due to the relative abundance

of CRTH2 in β-cells and its absence from other endocrine cell-types and the acinar pancreas, CRTH2 has emerged as a novel target for imaging of BCM in diabetes research.[10, 11] The possibility to study BCM *in vivo* using a noninvasive imaging technique such as Positron Emission Tomography (PET) would greatly contribute to the basic understanding of the processes surrounding diabetes and could also be pivotal in drug development, for example as a diagnostic tool for clinical trial inclusions and treatment follow-up.

Since the discovery of the NSAID indomethacin as a CRTH2 ligand in 2002[12] there has been an enormous amount of work directed towards the design and synthesis of small-molecule CRTH2 antagonists.[13] MK-7246 (Scheme 1) is a potent and selective CRTH2 antagonist developed by Merck for the treatment of respiratory disease[14, 15] structurally related to the dual thromboxane/CRTH2 antagonist ramatroban and the selective CRTH2 antagonist TM30089. In addition to receptor binding and selectivity, MK-7246 was also reported to possess good pharmacokinetic properties across a range of species and was subsequently evaluated in phase I clinical trials. Based on this and the feasibility for carbon-11 radionuclide incorporation, we identified the MK-7246 structure as a promising tracer candidate for PET-imaging of the CRTH2 receptor distribution *in vivo* both as a surrogate marker for BCM and to study target engagements with potential drug compounds.

Radionuclide incorporation was envisioned through methylation of a novel *N*-desmethyl-*O*-methyl MK-7246 precursor using [^{11}C]methyl iodide (Scheme 1). While *N*-methylation of sulfonamides is a common strategy in organic synthesis,[16] there are surprisingly few radiochemistry applications where [^{11}C]methyl iodide is used.[17, 18] Herein, we describe the synthesis and initial preclinical evaluation of [^{11}C]MK-7246.

2 **Materials and methods**

2.1 General information

Analytical thin-layer chromatography (TLC) was performed on silica gel 60 F-254 plates and visualized with UV light. Flash column chromatography was performed on silica gel 60 (40-63 μm). ^{1}H and ^{13}C spectra were recorded at 400 and 100 MHz, respectively and the chemical shifts

for ^{1}H NMR and ^{13}C NMR are referenced to TMS via residual solvent signals (^{1}H: MeOD at 3.31 ppm, $CDCl_3$ at 7.26 ppm and DMSO-d_6 at 2.50 ppm; ^{13}C: MeOD at 49.0 ppm, $CDCl_3$ at 77.0 ppm and DMSO-d_6 at 39.5 ppm). Analytical HPLC/ESI-MS was performed using electrospray ionization (ESI) and a C18 column (50×3.0 mm, 2.6 µm particle size, 100 Å pore size) with acetonitrile/water in 0.05% aqueous formic acid as mobile phase at a flow rate of 1.5 mL/min. UV-HPLC purity analyses were performed using a C18 column with a gradient of 5-100% acetonitrile/water in 0.05% aqueous formic acid as mobile phase with a flow rate of 1.5 mL/min for 5 mins unless otherwise stated. High resolution molecular masses (HRMS) were determined on a mass spectrometer equipped with an ESI source and time-of-flight (TOF) mass analyzer.

*2.2 2-(2-((tert-butyldimethylsilyl)oxy)ethyl)-1-((4-fluorophenyl)sulfonyl)aziridine **(3)***

The title compound was synthesized from commercially available D-aspartic acid according to a literature procedure (Scheme 2).[19]

*2.3 Methyl 2-(1-(2-((4-fluorophenyl)sulfonamido)-4-hydroxybutyl)-1H-indol-3-yl)acetate **(5)***

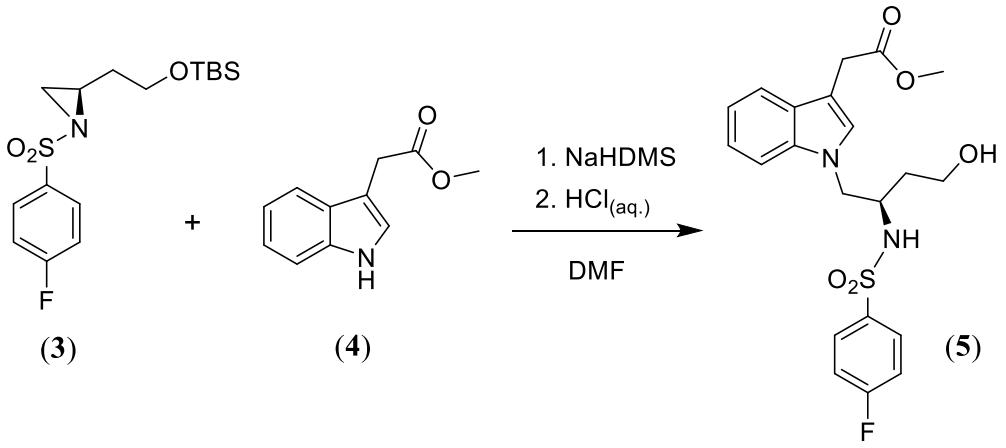

To a stirred solution of methyl 2-(1H-indol-3-yl)acetate **4** (1.05 g, 5.55 mmol, 1.0 equiv) in dry DMF (5 mL), a solution of NaHDMS (1.0 M in THF) was added dropwise over 30 min (5.56 mL, 5.56 mmol, 1.0 equiv) at 0 °C under nitrogen atmosphere. After 15 min, a solution of 2-(2-((tert-butyldimethylsilyl)oxy)ethyl)-1-((4-fluorophenyl)sulfonyl)aziridine **3** (1.00 g, 2.78 mmol,

0.5 equiv) in dry DMF (5 mL) was added dropwise over 40 min to the reaction mixture and stirred for another 1 h. The reaction mixture was then treated dropwise over 30 min with 2 M aq. HCl (10 mL). After 1.5 h, the mixture was diluted with satd. brine (5 mL) and the aqueous layer was extracted with EtOAc (3 x 10 mL). The combined organic layer was washed with brine (30 mL), dried over anhydrous $MgSO_4$ and concentrated under reduced pressure. The residue was purified by flash column chromatography (30 to 100 % EtOAc in hexane) to give the title compound as a yellow viscous liquid (682 mg, 56 %). ^{1}H NMR (400 MHz, Chloroform-*d*) δ 7.60–7.50 (m, 2H), 7.47 (dt, *J* = 7.8, 1.0 Hz, 1H), 7.21–7.05 (m, 3H), 6.91 (d, *J* = 1.0 Hz, 1H), 6.88–6.80 (m, 2H), 5.87 (d, *J* = 7.7 Hz, 1H), 4.14–3.98 (m, 2H), 3.93–3.73 (m, 1H), 3.71 (s, 3H), 3.65 (d, *J* = 0.8 Hz, 2H), 3.61–3.41 (m, 1H), 2.66 (s, 1H), 1.74 (ddt, *J* = 14.3, 8.5, 4.3 Hz, 1H), 1.50 (dddd, *J* = 14.5, 9.2, 5.5, 3.7 Hz, 1H). ^{19}F NMR (376 MHz, $CDCl_3$) δ -105.09. ^{13}C NMR (101 MHz, $CDCl_3$) δ 172.8, 164.7 (d, *J* = 254.3 Hz), 136.3, 135.6 (d, *J* = 3.2 Hz), 129.2 (d, *J* = 9.0 Hz), 127.8, 127.2, 122.2, 119.6, 119.1, 115.8 (d, *J* = 23.4 Hz), 109.4, 107.5, 58.8, 52.3, 52.1, 50.5, 35.0, 30.1. HRMS calcd for $C_{21}H_{24}N2O_5FS$ $[M + H]^+$ 435.1390, found 435.1395.

2.4 Methyl 2-(1-(2-((4-fluorophenyl)sulfonamido)-4-oxobutyl)-1H-indol-3-yl)acetate ***(5a)***

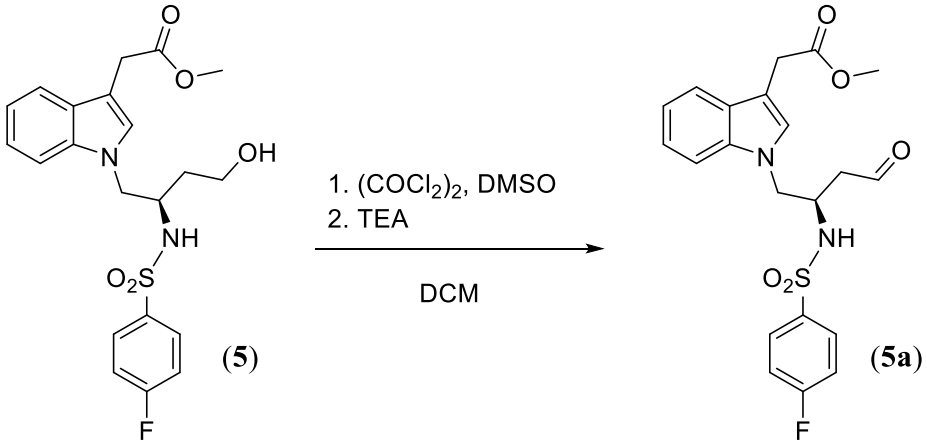

Dry DMSO (0.28 mL, 3.93 mmol, 2.5 equiv) was added dropwise to a stirred solution of oxalyl chloride (0.16 mL, 1.88 mmol, 1.2 equiv) in dry DCM (5 mL) at -60 °C under nitrogen atmosphere. After 30 min, a solution of **5** (682 mg, 1.57 mmol, 1.0 equiv) in dry DCM (5 mL) was added dropwise and reaction was stirred for a further 30 min. The reaction mixture was then treated with Et_3N (0.88 mL, 6.28 mmol, 4.0 equiv), warmed up to room temperature and stirred for 3 h. The

reaction was quenched with saturated $NaHCO_{3(aq.)}$ (5 mL), the layers were separated, and the aqueous layer was extracted with DCM (2 x 5 mL). The combined organic layer was washed with brine (10 mL), dried over anhydrous $MgSO_4$ and filtered through a silica pad. The solvent was removed from the filtrate under reduced pressure to give the crude title compound as yellow foam.

*Note: The aldehyde **5a** was immediately used for the next step without any purification due to poor stability.*

2.5 Methyl 2-(7-((4-fluorophenyl)sulfonamido)-6,7-dihydropyrido[1,2-a]indol-10-yl)acetate ***(6)***

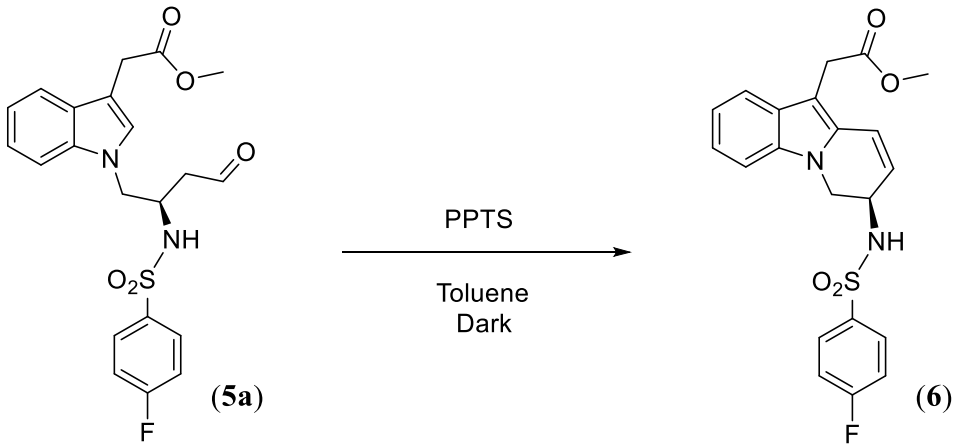

To a stirred solution of crude aldehyde **5a** (651 mg, 1.57 mmol, 1.0 equiv) in toluene (10 mL) was added PPTS (120 mg, 0.41 mmol, 0.26 equiv). The vial was protected from light and the reaction mixture was stirred at 60 °C overnight. The reaction mixture was diluted with water (10 mL) and the aqueous layer was extracted with EtOAc (2 x 10 mL). The combined organic layer was washed with brine (20 mL), dried over anhydrous $MgSO_4$ and concentrated under reduced pressure. The residue was purified by flash column chromatography (20 – 50 % EtOAc in hexane) to give the title compound as yellow solid (300 mg, 45 %). ^{1}H NMR (400 MHz, Chloroform-*d*) δ 7.91 (ddd, *J* = 8.9, 5.0, 2.4 Hz, 2H), 7.58 (dt, *J* = 8.0, 1.0 Hz, 1H), 7.21 (dd, *J* = 9.0, 8.2 Hz, 2H), 7.16–7.06 (m, 2H), 6.76 (dd, *J* = 9.8, 0.9 Hz, 1H), 5.73 (dd, *J* = 9.8, 5.3 Hz, 1H), 4.87 (d, *J* = 8.9 Hz, 1H), 4.51–4.31 (m, 1H), 4.19 (dd, *J* = 12.7, 4.0 Hz, 1H), 3.99 (dd, *J* = 12.7, 4.6 Hz, 1H), 3.74 (d, *J* = 1.1 Hz, 2H), 3.67 (s, 3H). ^{19}F NMR (376 MHz, $CDCl_3$) δ -104.59. ^{13}C NMR (101 MHz, $CDCl_3$) δ 171.8,

165.3 (d, *J* = 255.5 Hz) 137.2, 130.7, 129.7 (d, *J* = 9.0 Hz), 128.2, 123.5, 122.3, 121.2, 120.3, 119.5, 116.8 (d, *J* = 21.8 Hz), 108.9, 106.7, 52.2, 47.6, 46.3, 29.8. HRMS calcd for $C_{21}H_{20}N_2O_4FS$ $[M + H]^+$ 415.1128, found 415.1117.

*2.6 Methyl 2-(7-((4-fluorophenyl)sulfonamido)-6,7,8,9-tetrahydropyrido[1,2-a]indol-10-yl)acetate **(1)***

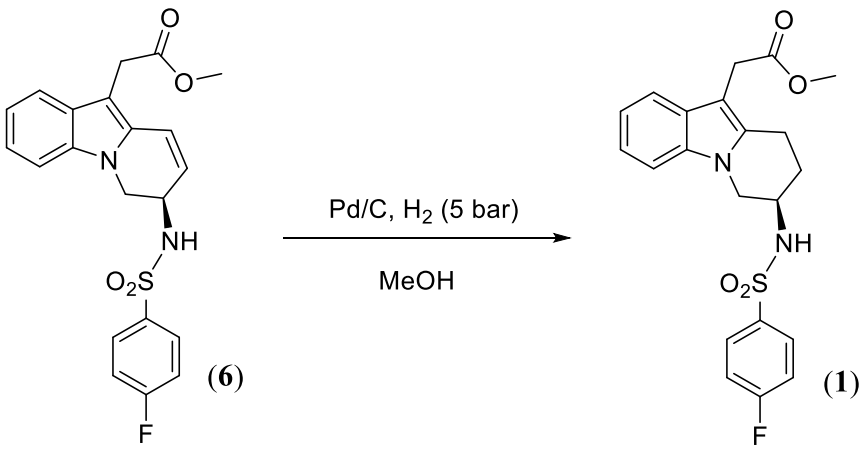

To a stirred solution of **6** (60 mg, 0.15 mmol, 1.0 equiv) in MeOH (3 mL) was added Pd/C (10 %, 6 mg). The vial was purged with hydrogen three times and stirred under a 5 bar atmosphere for 24 h. The reaction mixture was filtered through celite and the solvent was evaporated under reduced pressure. The residue was purified by flash column chromatography (hexane: EtOAc, 2:1) to yield the title compound as yellow solid (50 mg, 80 %). ^{1}H NMR (400 MHz, Chloroform-*d*) δ 7.94–7.84 (m, 2H), 7.57–7.48 (m, 1H), 7.21–7.09 (m, 4H), 7.08–7.04 (m, 1H), 5.10 (d, *J* = 8.0 Hz, 1H), 4.10 (dd, *J* = 11.8, 4.5 Hz, 1H), 3.97–3.86 (m, 1H), 3.75 (dd, *J* = 11.8, 6.5 Hz, 1H), 3.65 (s, 3H), 3.64 (s, 2H), 3.08–2.85 (m, 2H), 1.99–1.79 (m, 2H). ^{19}F NMR (376 MHz, $CDCl_3$) δ -104.60. ^{13}C NMR (101 MHz, $CDCl_3$) δ 172.4, 165.2 (d, *J* = 252.2 Hz), 163.9, 136.7 (d, *J* = 3.2 Hz), 135.7, 132.0, 129.7 (d, *J* = 9.5 Hz), 128.0, 121.2, 120.2, 118.1, 116.5 (d, *J* = 21.5 Hz), 108.6, 103.2, 52.0, 48.4, 47.4, 29.9, 27.0, 19.0. HRMS calcd for $C_{21}H_{22}N_2O_4FS$ $[M + H]^+$ 417.1284, found 417.1286.

2.7 General Information – Radiosynthesis

All reagents were purchased at high commercial quality and used without further purification. Transfer gas helium 5.0 and target gas nitrogen/0.05% oxygen mixture for ^{11}C-radionuclide production were purchased from AGA (Sweden). Disposable reaction vials (crimp neck, conical 0.9 mL) were purchased from VWR (Sweden) and capping septum (1.5 mm, 11 mm aluminium crimp cap, silicone/PTFE seal) was purchased from Scantec Nordic (Sweden). All presented radiochemical yields are decay corrected. The synthesis was automated using Tracer Production System (TPS) built in-house. Purification was performed by semi-preparative high-performance liquid chromatography (VWR LaPrep) equipped with pump (LP-1200), UV detector (Detector 40D), radiodetector (Flow-Count PMT, Bioscan), auto-sampler (TPS, built in-house) and a column. The effluent was monitored using UV detector (254 nm) and radiodetector. The radiochemical purity and identities of the labelled products were assessed by analytical HPLC (VWR LaChrom Elite) equipped with an auto-sampler (L-2200), pump (L-2130), diode array detector (L-2450), radiodetector (Flow-Count PMT, Bioscan).

2.8 Synthesis of [^{11}C]MK-7246

Cyclotron produced [^{11}C]carbon dioxide was transferred in helium gas and trapped in a solution of $LiAlH_4$ (300 µL, 0.1 M) in tetrahydrofuran. The solvent was removed under a stream of nitrogen (160 mL/min) while heating at 80 °C during 2 min. Hydriodic acid (600 µL, 57%) was added through a septum to the vessel which inlet and outlet was closed by a valve. The vessel was then heated at 130 °C for 70 s and subsequently cooled to 80 °C before the formed [^{11}C]methyl iodide was transferred in nitrogen gas (10 mL/min) over a phosphorous pentoxide/Ascarite column, into a septum equipped conical reaction vial where it was bubbled in a solution of *N*-desmethyl-*O*-methyl MK-7246 **1** (1.5 mg, 3.5 µmol) and NaH (1.2 mg, 50 µmol) in dimethylformamide (200 µL). The reaction mixture was heated at 90 °C for 3 min. The ester protecting group was then removed by the addition of aqueous NaOH (200 µL, 2 M) at 50 °C and heating at 80 °C for 5 min. The reaction mixture was then cooled to 50 °C, diluted and neutralized with $HCl_{(aq.)}$ (400 µL, 1 M) prior purification of the product by semi-preparative radio/UV-HPLC. Column: Phenomenex Kinetex 5µm C18 100 Å 150x10.0 mm; Eluent: A = ammonium formate 50 mM, pH 3.5; B =

acetonitrile; gradient elution 30-50% B @ 0-5 min with 4 mL/min flow rate. [^{11}C]MK-7246 eluted at 14 min, the collected fraction was transferred to a vortex evaporator where the eluent was removed, and the product was reformulated in phosphate buffered saline (4 mL, pH 7.4) and sterilized by filtration. The radiochemical purity was assessed by analytical HPLC and the identity was confirmed by co-elution with MK-7246 in a spiked sample. Analytical column: Chromolith Performance RP-18e, 100x4.6 mm; Eluent: A = water + 0.1% TFA; B = acetonitrile; gradient elution 5-73% B @ 0-8 min followed by column wash with 90% B, 4 mL/min flow rate.

2.9 In vitro autoradiography of [^{11}C]MK-7246 in pancreas

Human pancreatic biopsies collected from non-diabetic (n=4) and T2D (n=3) deceased donors were frozen to -80°C and processed into 20 µm slices. The use of human tissue was approved by the Uppsala Ethical Review Board (Dnr 2015-401; #2011/473, #Ups 02-577) and tissues obtained from Uppsala Biobank.

Sections were pre-incubated in 150 mL of 50 mM PBS (pH 7.4) + 1% BSA for 10 minutes. Radioactivity corresponding to approximately 0.04 (±0.01) MBq/mL [^{11}C]MK-7246 was added to the incubation buffer, and the sections were incubated at room temperature with radiotracer for 40 minutes. Non-displaceable binding was assessed by co-incubation with 20 µM MK-7246.

Following incubation, the tissue sections were washed 3 times for 3 minutes in 50 mM PBS at 4°C. The sections were dried and exposed to a digital phosphor-imager screen for 40 minutes (two radioactive half-lives). A reference of cross-calibrated radioactivity (measured in well-counter) was included to allow for quantification of the results. The screens were scanned using a Phosphorimager SI Typhoon (GE Healthcare). Adjacent pancreatic sections were separately stained for insulin (see details below).

2.10 Immuno-staining for insulin of frozen pancreas sections

Immunofluorescent (IF) staining for insulin was performed on pancreatic sections adjacent to those used for *in vitro* autoradiography binding studies. Briefly, sections were stained using Insulin A SC-7839 (Santa Cruz, Dallas, TX, USA; goat-polyclonal 1:1000). The sections were then incubated with secondary antibody Alexa fluor 488 (Invitrogen, Carlsbad, CA, USA; donkey anti-goat; dilution 1:100). Tile scan images were acquired with a Zeiss LSM780 confocal microscope. Images were analyzed in Zen Blue 2.0 (Carl Zeiss Microscopy GmbH, Germany).

2.11 Assessment of rat biodistribution by PET/MRI imaging

Rats (n=5, Sprague-Dawley, male, age 6-8 weeks; weight 277±47 g) were housed under standard laboratory condition with unlimited access to food and water. The animal experiments were approved by the Animal Research Ethical Committee of the Uppsala Region and were performed according to the Uppsala University guidelines on animal experimentation (UFV 2007/724). Animals were sedated by sevoflurane, controlled by an anesthesia vaporizer (3.0% sevoflurane) blended with 600 mL/min air/O_2 delivered through a face mask. The animals were placed in prone position on the heated bed of a small animal PET/ 3T MRI preclinical scanner (nanoScan, Mediso, Medical Imaging Systems, Budapest, Hungary). The breathing rate and body temperature were monitored by an integrated physiological monitoring system. The rats were administered 7.4±3.7 MBq [^{11}C]MK-7246 (maximum 300 µL volume) in the tail vein and examined by PET over the abdomen (field of view (FOV): 9.8cm) for up to 45-60 minutes. The list mode PET data was reconstructed into a dynamic sequence of 23 time-resolved images (12 frames x 10 s, 3 x 60 s, 5 x 300 s, 3 x 600 s) using a Tera tomo 3D algorithm (4 iterations, voxel size: 0.40 mm, matrix: 212×212x239).

A whole-body (WB) static PET examination was performed on each rat (3 bed-positions, 300s acquisition per bed position, reconstruction using Tera tomo 3D algorithm, 4 iterations, voxel size: 0.40 mm, matrix: 212x 212 x 582).

After the WB PET scan, a combination of MRI sequences was acquired over the abdomen to provide anatomic co-registration for organ segmentation (trans-axial and coronal T1W Spin Echo (SE), T2*W Gradient Echo (GRE), SE Multi FOV, T2W Fast SE).

PET and MRI images were analyzed using PMOD (version 3.510; PMOD Technologies Ltd.). Volumes of interest were drawn manually to include the adrenal, large intestine, small intestine, stomach, aorta, kidneys, liver, lung, muscle, pancreas, spleen, and urinary bladder in early or summed frames, and the dynamic time-activity uptake in each tissue was expressed as Standardized Uptake Values (SUV) by normalizing the uptake by the administered radioactive dose and animal weight.

2.12 Human predicted dosimetry of [^{11}C]MK-7246

The predicted dosimetry of [^{11}C]MK-7246 in human males was estimated based on the results from the rat biodistribution as assessed by PET/MRI imaging. The dosimetry calculations were performed as described previously.[20]

Briefly, SUV values in each tissue at several time points (20 s, 60 s, 120 s, 300 s, 600 s, 1200 s, 2400 s, 3600 s) were normalized to that of human tissues using tissue weights of a whole body adult reference male phantom.[21] The normalized SUVs were then un-decay corrected to their respective time point to reflect the actual radiation burden in each tissue and the residence time of [^{11}C]MK-7246 (MBq-h/MBq) in each tissue was calculated by trapezoidal approximation. The residence time from the last measured time point (60 min) until infinity in each tissue was estimated as mono-exponential decay of the nuclide (assuming negligible washout).

The absorbed dose in an adult reference male phantom (ICRP60) was calculated from the residence time in each tissue (OLINDA/EXM 1.1 software, VanderBilt University, Nashvillem USA). The organ specific doses are reported as mGy/ MBq (effective dose as mSv/MBq). The amount of MBq that can be safely administered annually (MBq/year) was calculated for each organ as well as the effective dose, by dividing the limiting dose (10 mSv/year for the effective dose, 150 mGy/year for all tissues except for red marrow with 50 mGy/year) by the absorbed dose per MBq (mGy/MBq or mSv/MBq).

2.13 Assessment of in vivo biodistribution and specificity in pig by PET/CT imaging

A high-health herd-certified pig (Yorkshire x Swedish Landrace x Hampshire, male, n=1, weight 24.7 kg) was examined by [^{11}C]MK-7246 PET/CT. The study was approved by the Animal Research Ethical Committee of the Uppsala Region and was performed according to the Uppsala university guidelines on animal experimentation (UFV 2007/724).

Anesthesia was maintained by intravenous infusion of ketamine, fentanyl and midazolam. The pigs were intubated through the trachea and with 30% oxygen in nitrogen. Oxygen saturation, HR, end-tidal carbon dioxide, ECG, arterial blood pressure and rectal body temperature were recorded throughout the examination. Fluid homeostasis was maintained with a continuous infusion of Ringer-acetate (Fresenius Kabi AB, Sweden). Glucose was added to the infusion anesthesia.

An arterial catheter was placed in the carotid artery for blood sampling and monitoring, and a central venous catheter was placed in the vena cava for radiopharmaceutical and blocking compound administration. Venous catheters were also placed in right and left auricular vein for anesthesia infusion.

The pig was examined 2 times during the experimental day in a Discovery MI PET/CT scanner (GE Healthcare). The pig was positioned with pancreas in the center of FOV of the PET/CT scanner by assistance of a scout CT scan. A dynamic PET sequence over 60 minutes was started simultaneously with each intravenous [^{11}C]MK-7246 administration. First, a baseline examination was performed following intravenous administration of 91.4 MBq [^{11}C]MK-7246. After 2 h (allowing for the carbon-11 to decay for several half-lives) a second examination was performed (IV 106.3 MBq [^{11}C]MK-7246) following 30 minutes intravenous pretreatment of 1 mg/kg MK-7246 to assess displaceable binding in pancreas and spleen.

The datasets were reconstructed into a 30 frames data set according to the following frame sequence: 12 x 10 s, 6 x 30 s, 5 x 2 min, 5 x 5 min, 2 x 10 min. Images were reconstructed using an iterative VPFX-S algorithm (GE Healthcare) (3 iterations, 16 subsets, and a 3 mm post-filter). A CT examination was used for attenuation correction.

Co-registered PET/CT images were analyzed in the Carimas software (Turku PET Center, Turku, Finland). All segmentations were performed on transaxial projections. To obtain the aortic signal,

single voxels were placed fully within the descending aorta on at least 10 transaxial projections, to minimize partial volume effects.

3 **RESULTS**

3.1 Synthesis of N-desmethyl-O-methyl MK-7246 ***(1)***

The synthesis of the precursor compound **1** is depicted in Scheme 3. The synthesis commenced with the nucleophilic ring opening of chiral aziridine **3**[19] with methyl ester protected indole **4**. Swern oxidation of the resulting alcohol **5** followed by acid-catalyzed cyclization of the aldehyde intermediate gave the cyclic alkene **6** in 45% yield. Finally, reduction of the alkene under elevated pressure (5 bar) in MeOH furnished the target precursor **1** in 80% yield.

3.2 Synthesis of [^{11}C]MK-7246 ***(2)***

After reformulation in phosphate buffered saline pH 7.4 (4 mL) and transfer to a sterile vial [^{11}C]MK-7246 was obtained in 5±2% radiochemical yield based on [^{11}C]methyl iodide. The radiochemical purity was 93±2% and the identity was confirmed by UV/radio-HPLC and co-elution with MK-7246 in a spiked sample, Figure 1.

3.3 In vitro autoradiography of [^{11}C]MK-7246 in pancreas

[^{11}C]MK-7246 binding in human pancreas was generally focal in nature and partially displaceable by addition of MK-7246, Figure 2(A).

The [^{11}C]MK-7246 focal binding was high in areas with higher density of insulin positive islet of Langerhans, in pancreas sections from non-diabetic individuals and individuals with T2D, Figure 2(B).

3.4 Assessment of rat biodistribution by PET/MRI imaging

[^{11}C]MK-7246 rapidly distributed into the blood pool after intravenous administration in rat, Figure 3(A) left panel and (B). First pass uptake was seen in lung in the early frames. Strong excretion by liver and to a lesser extent through the kidney was seen already after 2 minutes, Figure 3(A) middle panel. The hepatic uptake persisted throughout the PET/MRI examination. Radiometabolites were further excreted into the intestines likely through the biliary system, Figure 3(A) right panel. Most other tissues such as muscle exhibited very low background uptake combined with rapid washout.

3.5 Human predicted dosimetry of [^{11}C]MK-7246

[^{11}C]MK-7246 dosimetry calculation indicates the largest predicted human absorbed dose in the myocardium (heart wall) and liver, followed by small intestine, Figure 4(A). The absorbed dose to highly radio-sensitive tissues such as red marrow was relatively low. The whole body absorbed dose was 0.0036 mSv/MBq. Accordingly, the calculated acceptable annual dose in MBq of [^{11}C]MK-7246 was limited to maximally 2801 MBq based on the whole-body dose, Figure 4(B). All individual tissues tolerated in excess of 6000 MBq annually.

3.6 Assessment of in vivo biodistribution and specificity in pig by PET/CT imaging

In healthy pig [^{11}C]MK-7246 was rapidly distributed in the blood pool, Figure 5(A). First pass uptake in lungs was cleared within a few minutes. Strong early uptake was also seen in kidney and liver, Figure 5(B). The uptake in kidney also exhibited rapid clearance, while the hepatic uptake was displayed higher retention, Figure 5(C). After 20 minutes, the lumen of the small intestine showed strong uptake, Figure 5(D), which increased further at the end of the examination, Figure 5(E).

The pig pancreas and spleen, which express CRTH2,[11] displayed [^{11}C]MK-7246 baseline uptake (pancreas baseline SUV_{60min}=0.64, spleen baseline SUV_{60min}=1.15) which could be

abolished by pretreatment by 1 mg/kg MK-7246; pancreas pretreatment SUV_{60min}=0.21 (66% reduction), spleen pretreatment SUV_{60min}=0.14 (88% reduction), Figure 5(F-G). The concentration of [^{11}C]MK-7246 in aorta was not affected by the pretreatment; aorta baseline SUV_{60min}=0.25 and aorta pretreatment SUV_{60min}=0.26.

4 DISCUSSION

*4.1 Synthesis of N-desmethyl-O-methyl MK-7246 labeling precursor **(1)***

A comprehensive description of a number of medical chemistry and process orientated synthetic routes to MK-7246 have been previously described.[19] Although the manufacturing route proceeds through compound **1**, we did not have access to the key transaminase enzyme required for installing the amine functionality with the desired *(R)*-stereochemistry. Accordingly, we sought to develop an alternative synthetic route for the synthesis of the key precursor **1,** Scheme 3.

With previous efforts in mind, the aziridine-route was particularly attractive as it involves a chiral pool approach with the stereocenter originating from commercially available D-aspartic acid. In the original route, nucleophilic ring-opening of aziridine **3** was followed by installation of the *N*-methyl and an additional five synthetic steps to afford MK-7246. Due to the short half-life of ^{11}C, direct implementation of this approach to label MK-7246 was unfeasible and our strategy focused on allowing introduction of the *N*-methyl group as late as possible in the synthesis. Thus, the union of aziridine **3** and indole **4** was followed by concomitant protonation and TBS deprotection. Selective oxidation of the primary alcohol **5** led to the formation of aldehyde intermediate **5a**, which was found to be unstable and decomposed rapidly upon storage. To overcome this problem, the crude material was immediately advanced to the next step without purification. Treatment of crude **5a** with PPTS gave the desired alkene **6**, however this was accompanied by a competing intermolecular aldol condensation, which resulted in the moderate isolated yield (45%) obtained over the two-steps. In the final reduction step, our initial attempts using literature conditions[19] failed to produce any of the desired product. We suspected that this may be due to catalyst poisoning by the sulfonamide moiety, and gratifyingly the use of a protic solvent (MeOH) led to complete conversion of the alkene and afforded the labeling precursor **1** in 80% yield.

4.2 Synthesis of [^{11}C]MK-7246 ***(2)***

The two-step procedure to label [^{11}C]MK-7246 utilized conventional ^{11}C-methylation conditions using [^{11}C]methyl iodide followed by basic hydrolysis to remove the *O*-methyl protecting group. The protection group was introduced to ensure selective incorporation of the carbon-11 radioisotope at the sulfonamide nitrogen. [^{11}C]MK-7246 was synthesized using automated equipment and obtained with high radiochemical purity. The amount of activity in the product ready for injection was 270±120 MBq, the low radiochemical yield could in part be attributed to the moderately sterically encumbered secondary sulfonyl amide nucleophile. However, the obtained activity amount was enough for the current investigation involving *in vitro* assays and biodistribution/dosimetry in rat and pig. Further synthesis development will be carried out to increase the radiochemical yield to facilitate human studies.

4.3 Initial preclinical evaluation

Human pancreatic tissue was selected for the *in vitro* autoradiography assay, due to the potential of CRTH2 as a surrogate marker for BCM.[11] The focal [^{11}C]MK-7246 binding pattern was partially blockable (i.e. receptor mediated) and consistent with the heterogenous distribution of islets of Langerhans (as inferred from insulin staining), but also exhibited non-specific binding. On the other hand, the *in vivo* specificity in pig was very high, where >85% of the binding in CRTH2 rich spleen was displaceable. It is therefore likely that the *in vitro* autoradiography assay may overestimate the non-specific binding. This sort of technical difficulty for *in vitro* autoradiography (especially in pancreas) is not uncommon and may for example be due to high lipophilicity; [^{11}C]MK-7246 is indeed more lipophilic than previously published CRTH2 radioligand [^{11}C]AZ12204657.[11] Longer washing steps may alleviate this technical issue specific to the assay but is not practically possible when using the short-lived carbon-11 radionuclide. Thus, further assessment of *in vitro* specificity may focus on homogenate binding of pure islet and exocrine fractions from pancreas islet isolations, as well as on model cell lines expressing CRTH2.

Biodistribution in both rat and pig exhibited excretion mainly through the hepatic-biliary-intestinal axis, similar to previously evaluated CRTH2 specific radioligand [^{11}C]AZ12204657.[11] Strong

radioligand concentration in duodenum and jejunum may cause spillover of the PET signal into pancreas in small animals (e.g. mice or rats, and possibly non-human primates examined in clinical PET scanners), but this is not envisioned to pose a problem in pigs or in humans.

The rat biodistribution study was performed mainly for dosimetry calculation purposes. The rat as a diabetes model (i.e. measurement of BCM) is not ideal in this particular case as rat β-cells only express low levels of CRTH2 relative to pig, non-human primate or human.[10] Thus, the low uptake in rat pancreas observed in our studies is in agreement with previous studies of the same target. Instead, a pig model was used to probe the binding of [^{11}C]MK-7246 in pancreas. In pig, the spleen has been shown to bind another CRTH2 radioligand in a receptor mediated manner both *in vitro* and *in vivo*.[11] Consistent with these notions, [^{11}C]MK-7246 bound in both pig pancreas and spleen, in a manner that could be inhibited by pre-treatment by MK-7246. Of note, the magnitude of baseline uptake and the decrease in binding due to pretreatment was similar to that of [^{11}C]AZ12204657 indicating a similar mechanism.[11] Apart from being promising initial evidence for [^{11}C]MK-7246 as a potential marker of BCM, it also illustrates how [^{11}C]MK-7246 could be used as an indirect, quantitative target engagement marker for drugs targeting the CRTH2. Further large animal studies in pig and NHP are planned to repeat and confirm these findings.

[^{11}C]MK-7246 exhibited a safe human predicted dosimetry profile as extrapolated from the rat biodistribution data. Importantly, no particular tissue received a dose that would by itself limit the administration of the radioligand. Instead the whole-body dose was limiting, but still allowing for more than 2800 MBq [^{11}C]MK-7246 injected dose annually. Assuming a clinical dosing of 400 MBq [^{11}C]MK-7246 (approximately 5 MBq/kg), this potentially allows for up to 7 repeated PET examinations before reaching the 10 mSv yearly limit set for clinical research studies.

5 **Conclusions**

[^{11}C]MK-7246 was synthesized with high radiochemical purity in amounts sufficient for large animal PET studies. Initial preclinical *in vitro* and *in vivo* evaluation show promising binding, biodistribution and dosimetry properties. Further preclinical studies on [^{11}C]MK-7246 are warranted to assess its potential in applications such as BCM imaging and CRTH2 drug development.

Acknowledgments

The authors would like to thank JDRF, Science for Life Laboratory, the Knut and Alice Wallenberg Foundation, Diabetesfonden, Barndiabetesfonden, Vetenskapsrådet (2018-05133), and Göran Gustafssons Foundation for supporting the study. We would also like to thank the Preclinical PET/MRI Platform at Uppsala University.

FIGURES AND TABLES

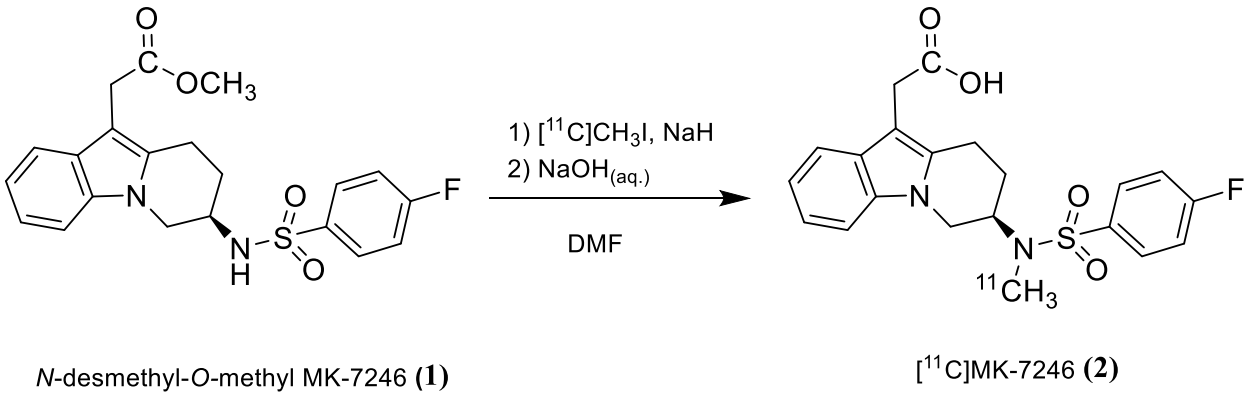

Scheme 1. *Synthesis of [^{11}C]MK-7246* ***(2)***.

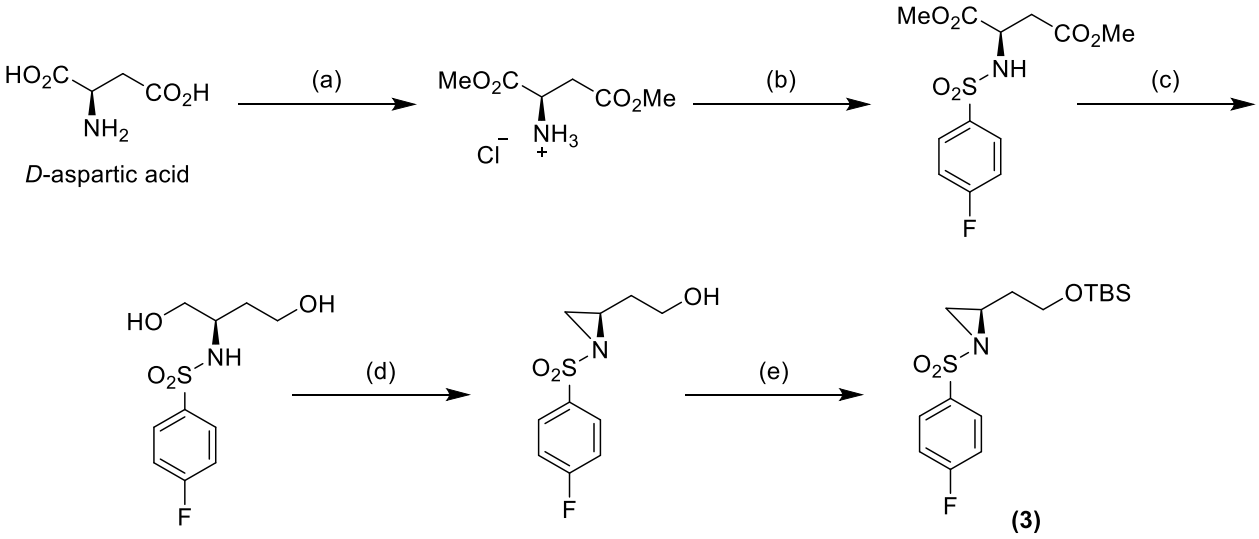

Scheme 2. *Synthesis of compound* ***3****. Reagents: (a) $SOCl_2$, MeOH (b) 4-Fluorobenzenesulfonyl chloride, TEA, THF (c) $NaBH_4$, EtOH; (d) ADDP, n-Bu_3P, THF (d) TBSCl, TEA, THF*

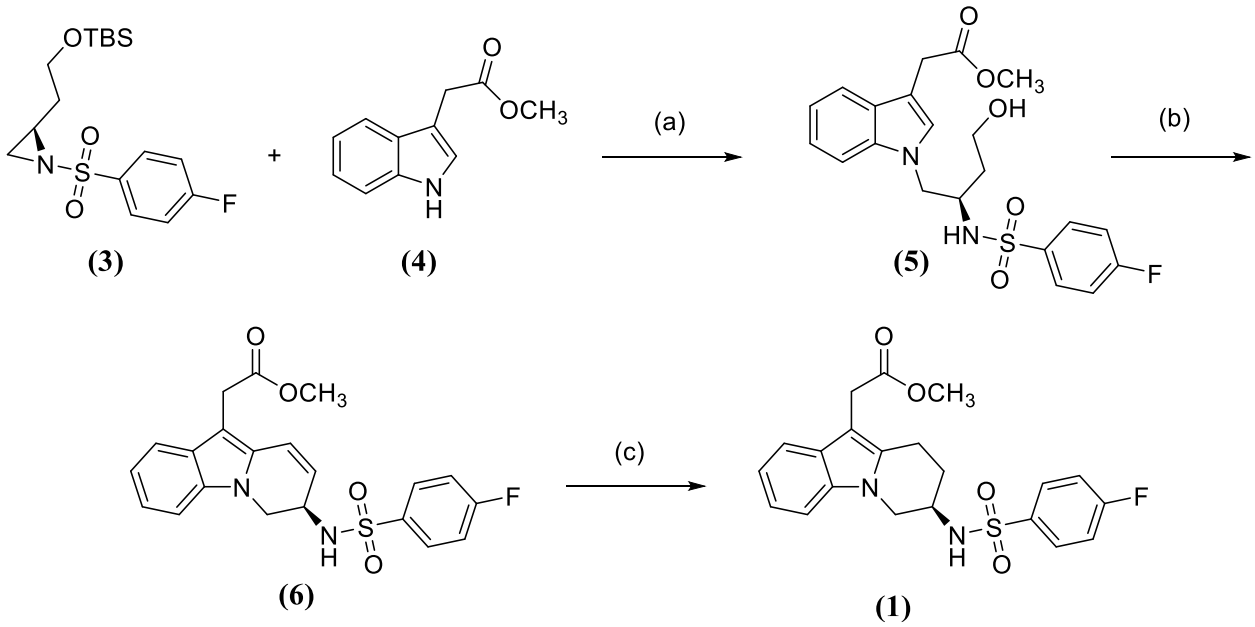

***Scheme 3**. Synthesis of N-desmethyl-O-methyl MK-7246 **(1)**. Reagents and conditions (a) i. **4**, NaHDMS, DMF, 0 °C, 15 min. ii. **3** DMF, 0 °C, 100 min. iii. $HCl_{(aq.)}$ 30 min, 56%. (b) i. DMSO, $(COCl_2)_2$, Et_3N, -60 °C to room temperature, 4 h; ii. PPTS, toluene, 60 °C to room temperature, 18 h, 45%. (c) Pd/C (10 %), H_2 (5 bar), MeOH, 24 h, 80%.*

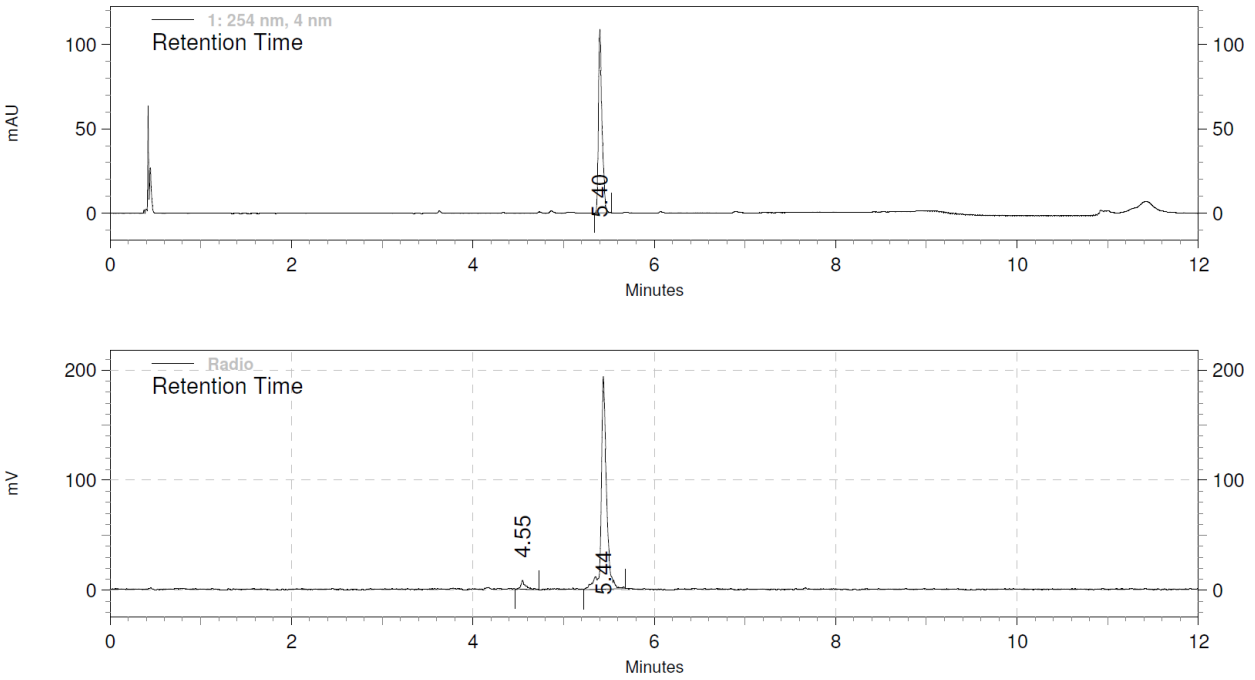

***Figure 1**. Radio/UV-HPLC analysis of sample taken from the [^{11}C]MK-7246 product solution and spiked with reference compound. Top: UV-trace with peak (5.40 min) corresponding to*

reference compound MK-7246. Bottom: Radio trace with peak (5.44 min) corresponding to [^{11}C]MK-7246.

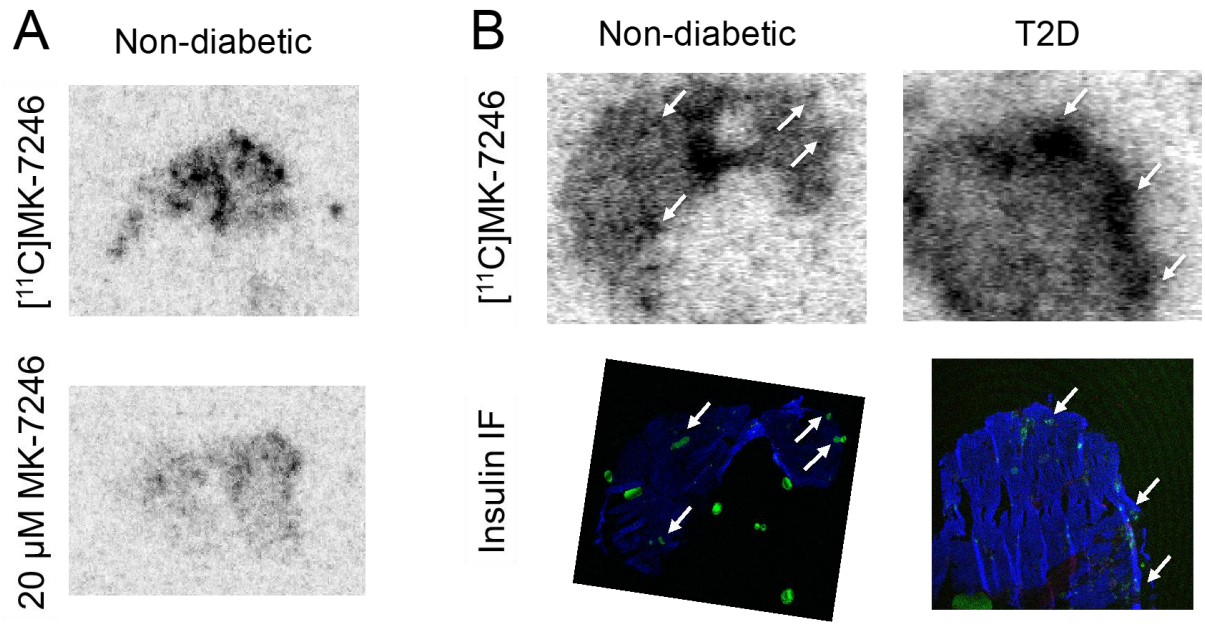

Figure 2. *(A) In vitro autoradiography in pancreas from non-diabetic human incubated either with [^{11}C]MK-7246 alone or co-incubated with 20 µM MK-7246. (B) [^{11}C]MK-7246 in vitro autoradiograms (top row) and immuno-fluorescent staining for insulin (bottom row) in adjacent pancreatic sections from non-diabetic (left panels) and T2D (right panels) individuals. White arrows indicate areas with insulin positive islets of Langerhans.*

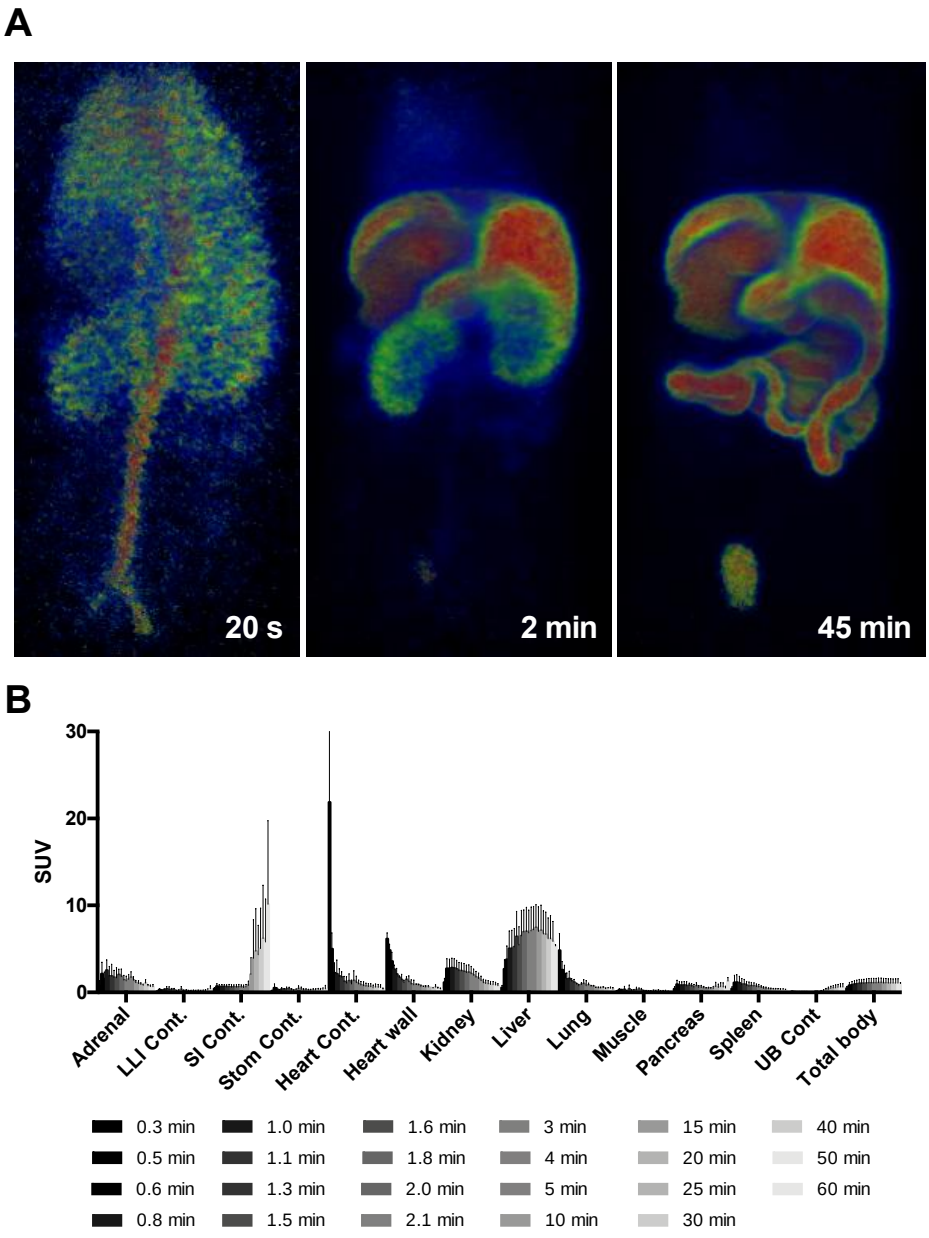

Figure 3. *(A) Biodistribution of [^{11}C]MK-7246 in rat as assessed by PET/MRI. Representative 3D projection images (coronal view) of biodistribution of [^{11}C]MK-7246 20 s, 2 min and 45 min after intravenous administration. Images are normalized to SUV=5. (B) Bar graph of uptake in tissues of interest for calculation of dosimetry.*

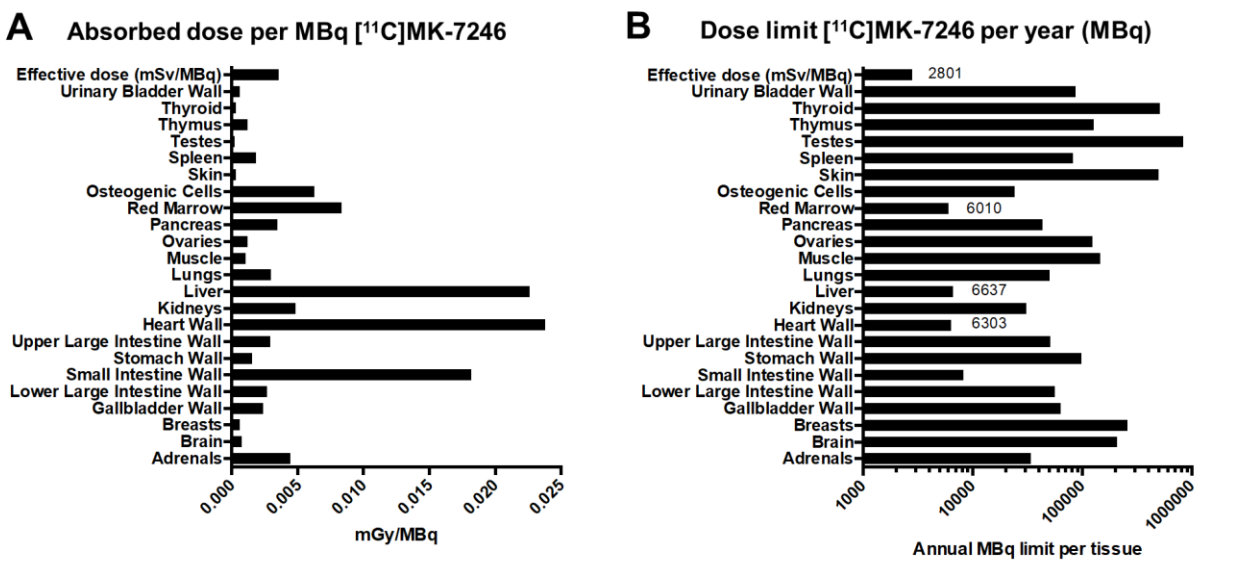

Figure 4. *Dosimetry of [^{11}C]MK-7246. (A) The absorbed radiation dose in relevant tissues per MBq of administered [^{11}C]MK-7246, as predicted in human based on dynamic rat biodistribution data. (B) The acceptable radioactive dose (in MBq) of [^{11}C]MK-7246 that can be administered per year in healthy subjects, as calculated from absorbed dose per tissue and the annual regulatory safety limit for each tissue.*

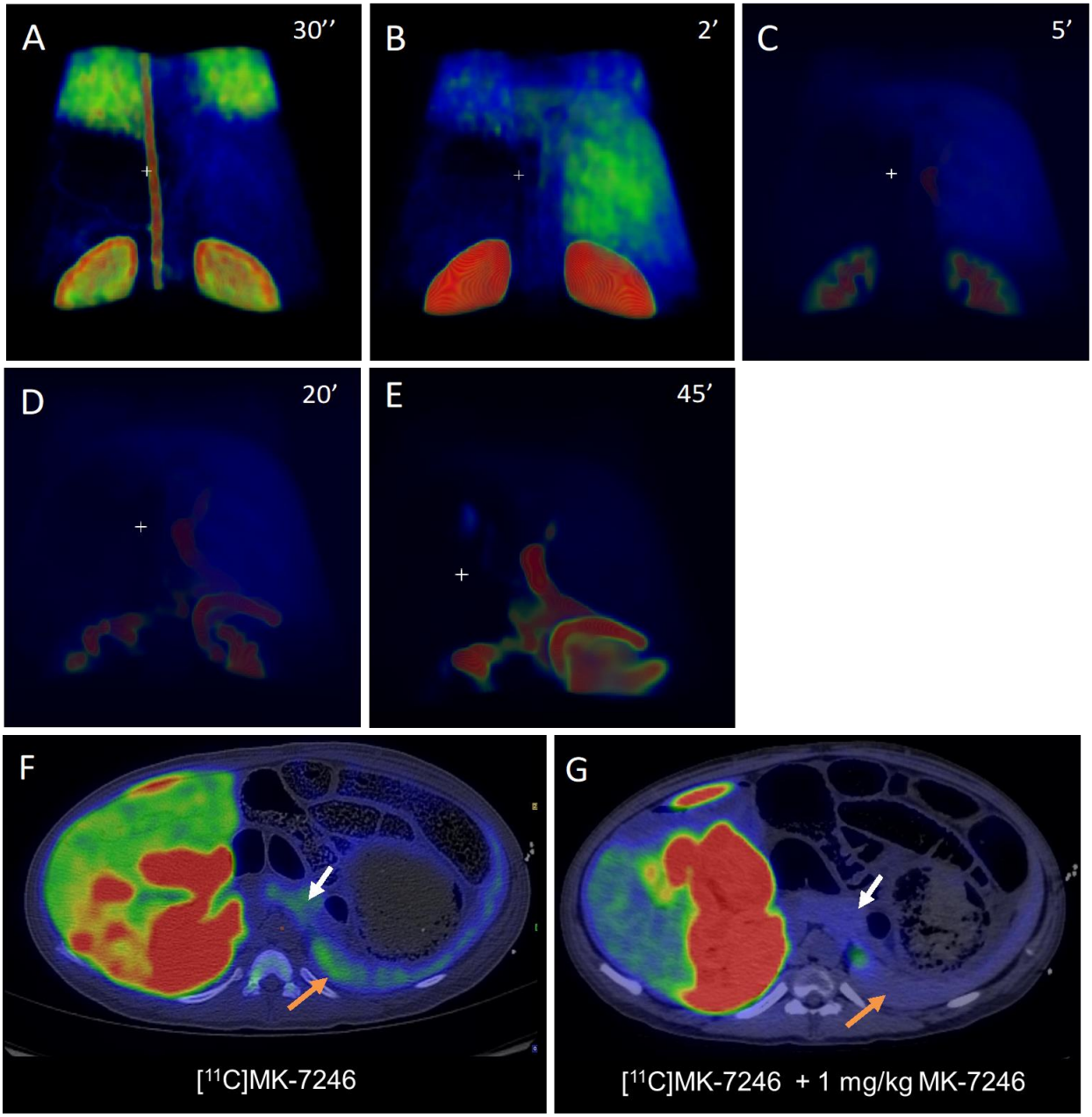

Figure 5. *3D projection images (coronal view) of biodistribution of [^{11}C]MK-7246 in pig assessed by PET/CT (A) 30 s, (B) 2 min, (C) 5 min, (D) 20 min and (E) 45 min after intravenous administration. Panels (A) and (B) are normalized to SUV=10, while panels (C), (D) and (E) are normalized to SUV=30. Transaxial projections normalized to SUV=3 showing the binding of [^{11}C]MK-7246 in CRTH2 rich tissues pancreas (white arrows) and spleen (orange arrows) at baseline (F) and after pretreatment with 1 mg/kg MK-7246 (G).*

REFERENCES

[1] Monneret G, Gravel S, Diamond M, Rokach J, and Powell WS. Prostaglandin D2 is a potent chemoattractant for human eosinophils that acts via a novel DP receptor. Blood 2001;98:1942-8.
[2] Gervais FG, Cruz RP, Chateauneuf A, Gale S, Sawyer N, Nantel F, et al. Selective modulation of chemokinesis, degranulation, and apoptosis in eosinophils through the PGD2 receptors CRTH2 and DP. J Allergy Clin Immunol 2001;108:982-8.
[3] Hirai H, Tanaka K, Yoshie O, Ogawa K, Kenmotsu K, Takamori Y, et al. Prostaglandin D2 selectively induces chemotaxis in T helper type 2 cells, eosinophils, and basophils via seven-transmembrane receptor CRTH2. J Exp Med 2001;193:255-61.
[4] Xue L, Gyles SL, Wettey FR, Gazi L, Townsend E, Hunter MG, et al. Prostaglandin D2 causes preferential induction of proinflammatory Th2 cytokine production through an action on chemoattractant receptor-like molecule expressed on Th2 cells. J Immunol 2005;175:6531-6.
[5] Shichijo M, Sugimoto H, Nagao K, Inbe H, Encinas JA, Takeshita K, et al. Chemoattractant receptor-homologous molecule expressed on Th2 cells activation in vivo increases blood leukocyte counts and its blockade abrogates 13,14-dihydro-15-keto-prostaglandin D2-induced eosinophilia in rats. J Pharmacol Exp Ther 2003;307:518-25.
[6] Xue L, Barrow A, and Pettipher R. Novel function of CRTH2 in preventing apoptosis of human Th2 cells through activation of the phosphatidylinositol 3-kinase pathway. J Immunol 2009;182:7580-6.
[7] Singh D, Ravi A, and Southworth T. CRTH2 antagonists in asthma: current perspectives. Clin Pharmacol 2017;9:165-73.
[8] Kupczyk M and Kuna P. Targeting the PGD2/CRTH2/DP1 Signaling Pathway in Asthma and Allergic Disease: Current Status and Future Perspectives. Drugs 2017;77:1281-94.
[9] Lindskog C, Korsgren O, Pontén F, Eriksson JW, Johansson L, and Danielsson A. Novel pancreatic beta cell-specific proteins: antibody-based proteomics for identification of new biomarker candidates. J Proteomics 2012;75:2611-20.
[10] Hellström-Lindahl E, Danielsson A, Ponten F, Czernichow P, Korsgren O, Johansson L, et al. GPR44 is a pancreatic protein restricted to the human beta cell. Acta Diabetol 2016;53:413-21.
[11] Eriksson O, Johnström P, Cselenyi Z, Jahan M, Selvaraju RK, Jensen-Waern M, et al. In Vivo Visualization of β-Cells by Targeting of GPR44. Diabetes 2018;67:182-92.
[12] Hirai H, Tanaka K, Takano S, Ichimasa M, Nakamura M, and Nagata K. Cutting edge: agonistic effect of indomethacin on a prostaglandin D2 receptor, CRTH2. J Immunol 2002;168:981-5.
[13] Norman P. Update on the status of DP2 receptor antagonists; from proof of concept through clinical failures to promising new drugs. Expert Opin Investig Drugs 2014;23:55-66.
[14] Gervais FG, Sawyer N, Stocco R, Hamel M, Krawczyk C, Sillaots S, et al. Pharmacological characterization of MK-7246, a potent and selective CRTH2 (chemoattractant receptor-homologous molecule expressed on T-helper type 2 cells) antagonist. Mol Pharmacol 2011;79:69-76.
[15] Gallant M, Beaulieu C, Berthelette C, Colucci J, Crackower MA, Dalton C, et al. Discovery of MK-7246, a selective CRTH2 antagonist for the treatment of respiratory diseases. Bioorg Med Chem Lett 2011;21:288-93.
[16] Nordeman P, Estrada S, Odell LR, Larhed M, and Antoni G. (11)C-Labeling of a potent hydroxyethylamine BACE-1 inhibitor and evaluation in vitro and in vivo. Nucl Med Biol 2014;41:536-43.
[17] Wang M, Lacy G, Gao M, Miller KD, Sledge GW, and Zheng QH. Synthesis of carbon-11 labeled sulfonanilide analogues as new potential PET agents for imaging of aromatase in breast cancer. Bioorg Med Chem Lett 2007;17:332-6.
[18] Wang M, Gao M, Miller KD, Sledge GW, Hutchins GD, and Zheng Q-H. Radiosynthesis of New Carbon-11-labeled Nimesulide Analogs as Potential PET SAER Tracers for Imaging of Aromatase Expression in Breast Cancer. Synth. Commun. 2010;40:749-58.

[19] Molinaro C, Bulger PG, Lee EE, Kosjek B, Lau S, Gauvreau D, et al. CRTH2 antagonist MK-7246: a synthetic evolution from discovery through development. J Org Chem 2012;77:2299-309.
[20] Selvaraju RK, Bulenga TN, Espes D, Lubberink M, Sörensen J, Eriksson B, et al. Dosimetry of [(68)Ga]Ga-DO3A-VS-Cys(40)-Exendin-4 in rodents, pigs, non-human primates and human - repeated scanning in human is possible. Am J Nucl Med Mol Imaging 2015;5:259-69.
[21] Cristy M and Eckerman K. Specific absorbed fractions of energy at various ages from internal photon sources. VI. Newborn. ORNL/TM-8381 1987;6.